Frequency-bin entanglement with tunable phase

IOP Publishing Journal of Optics
J. Opt. 17 (2015) 105201 (5pp) doi:10.1088/2040-8978/17/10/105201

Frequency-bin entanglement with tunable phase

Xianxin Guo, Peng Chen, Chi Shu, M M T Loy and Shengwang Du

Department of Physics, The Hong Kong University of Science and Technology, Clear Water Bay, Kowloon, Hong Kong, People's Republic of China

E-mail: dusw@ust.hk

Received 27 April 2015, revised 16 June 2015
Accepted for publication 22 June 2015
Published 24 September 2015

Abstract

We describe a technique to produce narrow-band photon pairs with frequency-bin entanglement, whose relative phase can be tuned using linear polarization optics. We show that, making use of the polarization-frequency coupling effect, the phase of a complex polarizer can be transferred into the frequency entanglement.

Keywords: entanglement, frequency-bin, quantum information

Entanglement is an essential part of the nature of compound quantum systems [1, 2]. For wide-band photon pairs produced from spontaneous parametric down conversion (SPDC) in a nonlinear crystal, entanglement between discrete frequency bands can be manipulated with a dispersive prism pair and a spatial light modulator [3, 4]. However, this method cannot be applied to narrow-band biphotons whose bandwidth is in the order of 10 MHz. Zeilinger *et al* showed that the polarization entanglement can be transferred into frequency using a polarizing beam splitter (PBS) and polarization projections [5]. In this configuration, the phase adjustment is done in the polarization entanglement before the PBS.

Here we describe a different approach to create narrow-band frequency entanglement with tunable phase. Following our recent demonstration of generating narrow-band biphotons with polarization-frequency-coupled hyperentanglement, we find that it is possible to transfer the polarization-induced phase into that of the frequency entanglement [6]. Different from the work by Zeilinger *et al* [5], our scheme does not require an initial polarization entanglement from the source. We make use of the polarization-frequency coupling to transfer the phase of a complex polarizer into the frequency entanglement.

The schematic of our experimental setup and related atomic energy level diagram are depicted in figure 1. We produce narrow-band biphotons from spontaneous four-wave mixing (SFWM) in a laser-cooled ^{85}Rb atomic ensemble with a right-angle geometry [7]. The coupling laser (ω_c, 3 mW, diameter 2 mm) is on resonance with the transition $|2\rangle \rightarrow |3\rangle$, and the pump laser ($\omega_p$, 40 mW diameter 2 mm) is far blue detuned from the transition $|1\rangle \rightarrow |3\rangle$ by $\Delta_p = 2\pi \times 3033$ MHz. With the counter-propagating pump and coupling laser beams, phase-matched backward paired Stokes (ω_s) and anti-Stokes (ω_{as}) photons are spontaneously produced with exchange symmetry in paths 1 and 2: Stokes photons go to path 1 and anti-Stokes photons to path 2, and vice versa. To ensure there is no polarization entanglement pre-required in our configuration, we pass both ports (1 and 2) to horizontal (H) linear polarizers. Then we shift the optical angular frequencies of the photons in path 1 by $\delta = 2\pi \times 100$ MHz using an acousto-optical modulator (AOM), and adjust the photons in path 2 to be vertically (V) polarized using a half-wave plate (HWP). The photons from paths 1 and 2are incident to a 50:50 beam splitter (BS). The photons from the two output ports 3 and 4 of the BS pass through two polarizers (P_3 and P_4) and are detected by two single-photon counting modules (SPCMs) with a time-bin width of 1 ns. Further experimental details are described in [6].

In describing polarizations, we follow the convention where the wave is observed from the point of view of the source. The biphoton state output from the cold atoms can be described as

$$|\Psi_{1,2}\rangle = |HV\rangle \otimes \left(|\omega_s + \delta\rangle_1 |\omega_{as}\rangle_2 + |\omega_{as} + \delta\rangle_1 |\omega_s\rangle_2\right). \quad (1)$$

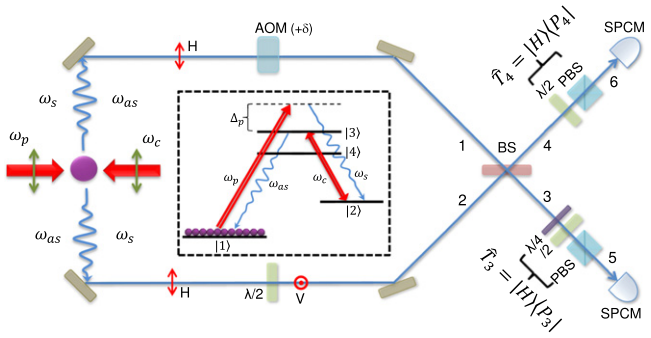

Figure 1. Schematic of experimental setup for producing narrow-band biphotons with frequency-bin entanglement. The phase-matched paired photons are generated from spontaneous four-wave mixing in laser-cooled ^{85}Rb atoms with a right-angle pump-coupling geometry. The relevant ^{85}Rb energy levels are $|1\rangle = |5S_{1/2}, F = 2\rangle$, $|2\rangle = |5S_{1/2}, F = 3\rangle$, $|3\rangle = |5P_{3/2}, F = 3\rangle$, and $|4\rangle = |5P_{3/2}, F = 2\rangle$.

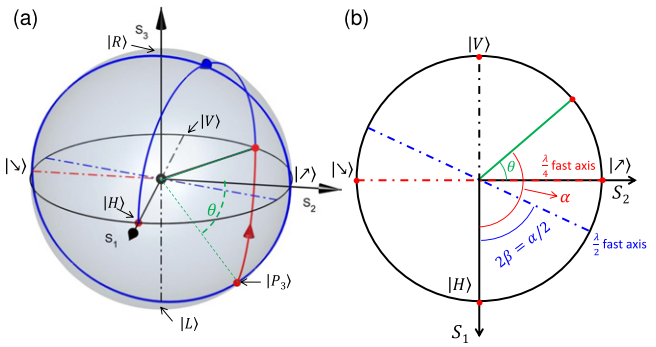

Figure 2. (a) The Poincaré sphere. An arbitrary projection state can be rotated to $|H\rangle$ with the combination of a half-wave plate and a quarter-wave plate. The blue (red) dash-dot line represents the rotation axis for the half-wave plate (quarter-wave plate), and the blue (red) arrow curve shows the half-wave plate (quarter-wave plate) rotation. (b) The equatorial S_1S_2-plane view.

In our setup there is no length difference between path 1 and path 2 before the BS. The BS has the transformation $\hat{a}_3 = (\hat{a}_{1\,\mathrm{H}} - \mathrm{i}\hat{a}_{2\,\mathrm{V}})/\sqrt{2}$, $\hat{a}_4 = (\mathrm{i}\hat{a}_{1\,\mathrm{H}} + \hat{a}_{2\,\mathrm{V}})/\sqrt{2}$. The two-photon state with the Stokes photon in output port 3 and the anti-Stokes photon in output port 4 is

$$|\Psi_{s3,as4}\rangle = \frac{1}{2}(|H, \omega_s + \delta\rangle_3|V, \omega_{as}\rangle_4 + |V, \omega_s\rangle_3|H, \omega_{as} + \delta\rangle_4), \quad (2)$$

which is a polarization-frequency-coupled entangled state [6]. Assuming the polarizers P_3 and P_4 in figure 1 have the operations $\hat{T}_3 = |H\rangle\langle P_3|$ and $\hat{T}_4 = |H\rangle\langle P_4|$, respectively, we can decouple the polarization degree of freedom by the polarization projection:

$$\begin{aligned}|\Psi_{s5,as6}\rangle &= \hat{T}_3\hat{T}_4|\Psi_{s3,as4}\rangle \\ &= \frac{1}{2}|HH\rangle \otimes (\langle P_3|H\rangle\langle P_4|V\rangle|\omega_s + \delta\rangle_3|\omega_{as}\rangle_4 \\ &\quad + \langle P_3|V\rangle\langle P_4|H\rangle|\omega_s\rangle_3|\omega_{as} + \delta\rangle_4). \end{aligned} \quad (3)$$

Setting $|\mathrm{P}_3\rangle = \frac{1}{\sqrt{2}}(|\mathrm{H}\rangle + (\mathrm{e}^{-i\theta}|\mathrm{V}\rangle)$ and $|\mathrm{P}_4\rangle = \frac{1}{\sqrt{2}}(|\mathrm{H}\rangle + |\mathrm{V}\rangle) = |\nearrow\rangle$, we obtain the (unnormalized) two-photon state

$$|\Psi_{s5,as6}\rangle = \tfrac{1}{4}|HH\rangle \otimes \left(|\omega_s + \delta, \omega_{as}\rangle + \mathrm{e}^{\mathrm{i}\theta}|\omega_s, \omega_{as} + \delta\rangle\right). \quad (4)$$

This is a frequency-bin entangled two-photon state whose relative phase difference θ is transferred from the phase difference between the polarization bases H and V of $|P_3\rangle$,

Now we turn to realizing the polarizer operations $\hat{T}_3$ and $\hat{T}_4$. It is known that in the polarization space, any two pure polarization states can be connected by the combination of a quarter-wave plate (QWP) and HWP. The polarizer operation $\hat{T}_4 = |H\rangle\langle\nearrow|$ can be realized by an HWP (with its fast axis aligned at 22.5° to H axis) and a PBS. For the complex polarizer operation $\hat{T}_3 = \frac{1}{\sqrt{2}}|H\rangle(\langle H| - \mathrm{e}^{\mathrm{i}\theta}\langle V|)$, we use the combination of a QWP, a HWP and a PBS to project the desired polarization $\mathrm{P}_3\rangle = \frac{1}{\sqrt{2}}(|\mathrm{H}\rangle - \mathrm{e}^{-\mathrm{i}\theta}|\mathrm{V}\rangle)$ to the $|H\rangle$ linearly polarized output of the PBS.

To illustrate this clearly, we plot the Poincaré sphere in figure 2. Any point on the Poincaré sphere represents a pure polarization state. Specifically, all linear polarization states are on the equator, with $|H\rangle$ and $|V\rangle$ at the intersections with S_1 axis, $|\nearrow\rangle = \frac{1}{\sqrt{2}}(|H\rangle + |V\rangle)$ and $|\searrow\rangle = \frac{1}{\sqrt{2}}(|H\rangle - |V\rangle)$ at the intersections with S_2 axis. The North Pole and South Pole represent the right-circular polarization $|R\rangle = \frac{1}{\sqrt{2}}(|H\rangle + \mathrm{i}|V\rangle)$ and the left-circular polarization $|L\rangle = \frac{1}{\sqrt{2}}(|H\rangle - \mathrm{i}|V\rangle)$, respectively. The projection state $|\mathrm{P}_3\rangle = \frac{1}{\sqrt{2}}(|\mathrm{H}\rangle + \mathrm{e}^{-\mathrm{i}\theta}\mathrm{V}\rangle)$ locates on the blue circle in the S_2S_3 plane. For a wave plate, its fast axis always locates on the equatorial plane and through the sphere centre, and the magnitude of rotation is determined by the phase retardance: 180 ° for an HWP and 90° for a QWP. We take the following two-step rotations to transfer the polarization state from $|\mathrm{P}_3\rangle = \frac{1}{\sqrt{2}}(|\mathrm{H}\rangle + \mathrm{e}^{-\mathrm{i}\theta}|\ \mathrm{V}\ \rangle)$ to $|H\rangle$. First, we rotate $|\mathrm{P}_3\rangle$ along the S_2 -axis (fast axis of the QWP) by 90° and it becomes a linear-polarization state in the S_1 S_2 plane with an angle $\alpha = \theta + \pi/2$ to the S_1 axis. Second, we set the fast axis of the HWP with an angle of $\alpha/2$ to the S_1 axis (i.e., we set the fast axis of the HWP with an angle of $\alpha/4 = \theta/4 + \pi/8$ to the H axis in the real space) and the intermediate polarization state is rotated to S_1 ($|H\rangle$). Therefore, to obtain the operation $\hat{T}_3 = \frac{1}{\sqrt{2}}|H\rangle(\langle H| + \mathrm{e}^{\mathrm{i}\theta}\langle V|)$, we set the fast axes of the QWP and HWP with $\pi/4$ and $\beta = \alpha/4 = \theta/4 + \pi/8$, respectively, to the horizontal (H) axis.

We can also verify the above transformations by obtaining the Jones matrix in the $\{|H\rangle, |\ V\rangle\}$ polarization bases:

$$\hat{T}_3(\beta) = |H\rangle\langle P_3| = \tfrac{1}{\sqrt{2}}\begin{bmatrix} 1 & \mathrm{e}^{\mathrm{i}(4\beta-\pi/2)} \\ 0 & 0 \end{bmatrix}, \quad (5)$$

and

$$\hat{T}_4 = |H\rangle\langle\nearrow| = \frac{1}{\sqrt{2}}\begin{bmatrix} 1 & 1 \\ 0 & 0 \end{bmatrix}, \tag{6}$$

To determine the phase $\theta = 4\beta - \pi/2$, we directly measure the two-photon beating in the time-domain. The two-photon temporal wave function can be obtained from equation (3):

$$\begin{aligned}\Psi_{56}(t_5, t_6) &= \langle HH; t_5, t_6|\Psi_{s5,as6}\rangle \\ &= \frac{1}{4}\psi_0(\tau)e^{-i\omega_s t_5}e^{-i\omega_{as}t_6}e^{-i\delta t_5}\Big[1 + e^{-i(\delta\tau-\theta)}\Big],\end{aligned} \tag{7}$$

where $\tau = t_6 - t_5$ and $\psi_0(\tau)e^{-i\omega_s t_5}e^{-i\omega_{as}t_6} = \langle t_5, t_6|\omega_s, \omega_{as}\rangle$ is the Stokes–anti-Stokes biphoton temporal wave function generated from the SFWM process [8]. The coincidence measurement of two-photons is related to the Glauber correlation function

$$\begin{aligned}G_{56}^{(2)}(\tau > 0) &= |\Psi_{56}(t_5, t_6)|^2 \\ &= \frac{1}{8}G_0^{(2)}(\tau)[1 + \cos(\delta\tau - \theta)\Big],\end{aligned} \tag{8}$$

where $G_0^{(2)}(\tau) = |\psi_0(\tau)|^2$ is the Glauber correlation function that can be measured before the BS. In the above discussion, we consider only Stokes photons in port 5 and anti-Stokes photons in port 6. Because of the system symmetry, Stokes photons can also appear in port 6 and anti-Stokes in port 5. Taking this into account, equation (8) is extended to $\tau < 0$ and becomes

$$G_{56}^{(2)}(\tau) = \frac{1}{8}G_0^{(2)}(|\tau|)[1 + \cos(\delta|\tau| - \theta)\Big]. \tag{9}$$

In figure 3(a), the red square data show the measured biphoton temporal envelope $G_0(|\tau|)$ before the BS, which agrees well with the theoretical result (red solid curve) following the perturbation theory [8]. The blue dots show the two-photon beating pattern of a frequency-bin entangled two-photon state measured at port 5 and port 6, with $\beta = 79°$, The normalized experimental beating pattern is shown in figure 3(b), from which we determine the relative phase $\theta_{exp} = (1.28 \pm 0.02)\pi$ by best fitting the data to a sine wave, which is consistent with $\theta = 4\beta - \pi/2$, We obtain a visibility of $(77 \pm 6)\%$, which is beyond the requirement for violating the Bell inequality [9]. Figure 3(c) shows the relative phase θ as a function of β, the angle of the fast axis of the HWP in $\hat{T}_3$. The phase values (circle points) obtained from the two-photon beating agree well with the theoretical prediction (solid line).

We further show that the amplitude ratio between the two frequency-bin components can be adjusted with this scheme. We take $|P_3\rangle = \frac{1}{\sqrt{2}}(|H\rangle + (e^{-i\theta}|V\rangle)$ and $|P_4\rangle = \cos\phi|H\rangle + \sin\phi|V\rangle$, then the non-maximally entangled two-photon state and Glauber correlation function at the output ports 5 and 6 become

$$\begin{aligned}|\Psi_{s5,as6}\rangle = \frac{1}{2\sqrt{2}}|HH\rangle \otimes (\cos\phi|\omega_s + \delta, \omega_{as}\rangle \\ + \sin\phi e^{i\theta}|\omega_s, \omega_{as} + \delta\rangle),\end{aligned} \tag{10}$$

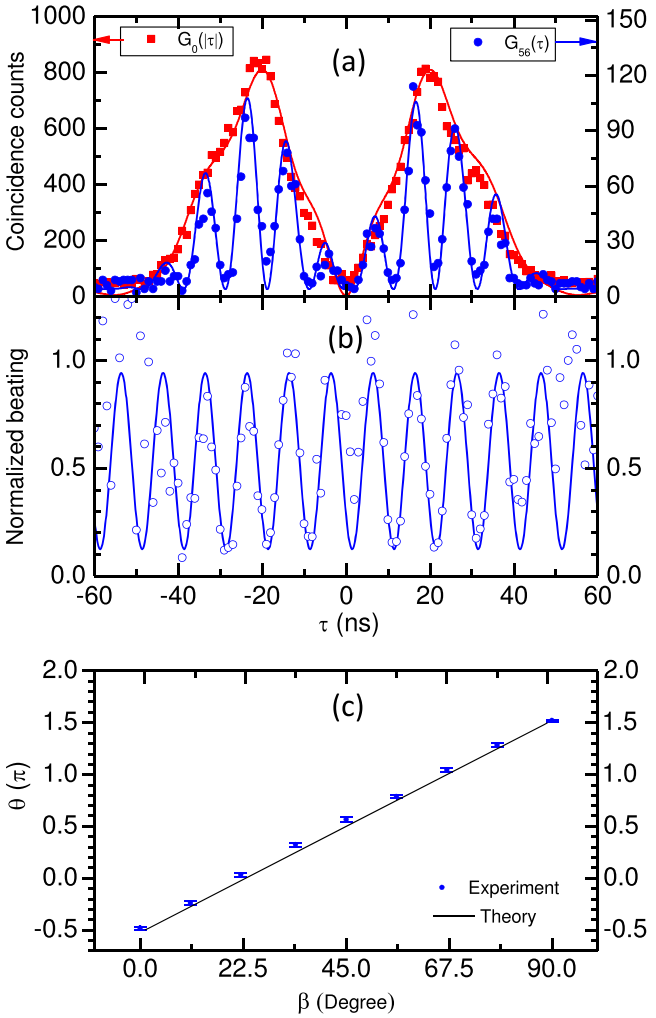

Figure 3. (a) The biphoton waveform $G_0(|\tau|)$ at ports 1 and 2 before BS and the two-photon beating pattern $G_{56}(\tau)$ measured at ports 5 and 6. We set $\beta = 79°$, which corresponds to $\theta = 1.25\pi$, (b) Normalized beating signal (blue circle) and sinusoidal fitting result (blue solid curve). The relative phase obtained from the fitted curve is $\theta_{exp} = (1.28 \pm 0.02)\pi$, (c) The relative phase θ of the frequency-bin entangled state as a function of the angle, β, between the fast axis of the HWP in $\hat{T}_3$ and the H axis. The phase values of the blue circles are obtained from sinusoidal fitting to the two-photon beatings. The black solid line is theoretically plotted from $\theta = 4\beta - \pi/2$,

$$G_{56}^{(2)}(\tau) = \frac{1}{8}G_0^{(2)}(|\tau|)[1 + \sin 2\phi\cos(\delta|\tau| - \theta)]. \tag{11}$$

The visibility of the normalized beating is reduced to $V = |\sin(2\phi)|$ due to the unbalanced amplitudes of the two bases. The experimental result under the condition of $\phi = \pi/12$ and $\theta = \pi$ is displayed in figure 4, with a measured visibility of $(51 \pm 5)\%$. It is obvious that any non-maximally entangled state with an arbitrary amplitude ratio can be easily prepared. These non-maximally entangled states are of particular interest to loophole-free tests of Bell inequalities since they reduce the required detector efficiencies [10–12]. In other situations where the maximally entangled state is favored, such amplitude adjustment also allows us to

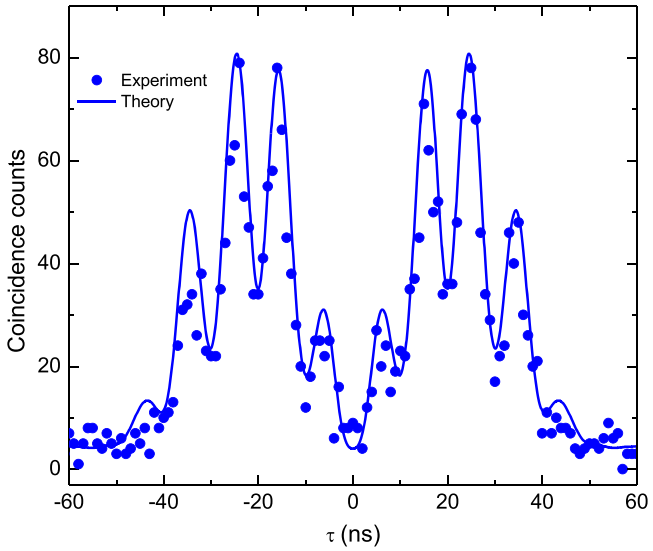

Figure 4. The two-photon beating with $\phi = \pi/12$ and $\theta = \pi$. The experimental visibility is $(51 \pm 5)\%$.

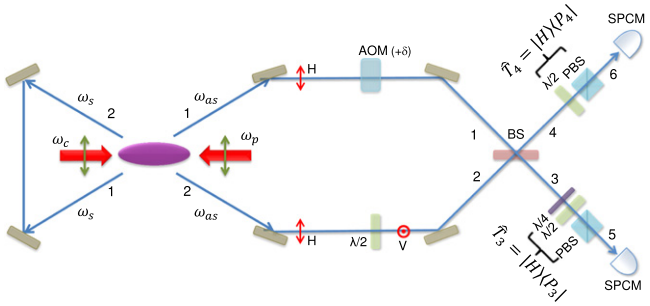

Figure 5. A possible experimental setup for generation of subnatural-linewidth frequency-bin entangled biphotons.

transform the non-maximally entangled state into a maximal one.

With our recently developed temporal quantum-state tomography [13], we measured our biphoton bandwidth to be about 20 MHz, which is insufficient for photon–atom interaction. Now we show that our scheme can be extended to create subnatural-linewidth frequency-bin entangled biphotons. In a typical 2D MOT system, which is popular for the generation of subnatural-linewidth biphotons [14–16], the biphoton collection paths only have a small angle with the pump-coupling path. We construct two biphoton collection paths symmetrically around the pump-coupling path, as shown in figure 5. The phase-matched Stokes and anti-Stokes photons go in different directions following the pump and coupling directions. Then we use two mirrors to reflect the Stokes photons in path 1 (2) back and overlap with the anti-Stokes in path 2 (1). After mixing the Stokes and anti-Stokes photons together, we can create frequency-bin entanglement following a similar procedure.

In conclusion, we have demonstrated a polarization-frequency-coupled scheme for generating controllable frequency-bin entangled narrow-band biphotons, whose relative phase and amplitude ratio between the entangled frequency bases can be arbitrarily tuned by adjusting the wave plates. Compared with the former schemes for wideband SPDC biphotons [3, 5, 17], our method only requires manipulating wave plates, which is more stable and versatile. Our technique can be easily extended to generate subnatural-linewidth frequency-bin entangled biphotons and find applications in realizing an efficient light-matter quantum interface in a quantum network [18].

The work was supported by the Hong Kong Research Grants Council (Project No. 16301214). C S acknowledges support from the Undergraduate Research Opportunities Program at the Hong Kong University of Science and Technology.

References

[1] Horodecki R, Horodecki P, Horodecki M and Horodecki K 2009 Quantum entanglement *Rev. Mod. Phys.* **81** 865–942
[2] Pan J-W, Chen Z-B, Lu C-Y, Weinfurter H, Zeilinger A and Zukowski M 2012 Multiphoton entanglement and interferometry *Rev. Mod. Phys.* **84** 777–838
[3] Bernhard C, Bessire B, Feurer T and Stefanov A 2013 Shaping frequency-entangled qudits *Phys. Rev.* A **88** 032322
[4] Peer A, Dayan B, Friesem A A and Silberberg Y 2005 Temporal shaping of entangled photons *Phys. Rev. Lett* **94** 073601
[5] Ramelow S, Ratschbacher L, Fedrizzi A, Langford N K and Zeilinger A 2009 Discrete tunable color entanglement *Phys. Rev. Lett.* **103** 253601
[6] Shu C, Guo X, Chen P, Loy M M T and Du S 2015 Narrowband biphotons with polarization-frequency coupled hyperentanglement *Phys. Rev.* A **91** 043820
[7] Liu C, Chen J F, Zhang S, Zhou S, Kim Y-H, Loy M M T, Wong G K L and Du S 2012 Twophoton interferences with degenerate and nondegenerate paired photons *Phys. Rev.* A **85** 021803(R)
[8] Du S, Wen J and Rubin M H 2008 Narrowband biphoton generation near atomic resonance *J. Opt. Soc. Am.* B **25** 98–108
[9] Clauser J F, Horne M A, Shimony A and Holt R A 1969 Proposed experiment to test local hidden-variable theories *Phys. Rev. Lett.* **23** 880
[10] White A G, James D F V, Eberhard P H and Kwiat P G 1999 Nonmaximally entangled states: Production, characterization, and utilization *Phys. Rev. Lett.* **83** 16
[11] Eberhard P H 1993 Background level and counter efficiencies required for a loophole-free Einstein-Podolsky–Rosen experiment *Phys. Rev.* A **47** R747
[12] Garuccio A 1995 Hardy's approach, Eberhard's inequality, and supplementary assumptions *Phys. Rev.* A **52** 2535
[13] Chen P, Shu C, Guo X, Loy M M T and Du S 2015 Measuring the biphoton temporal wave function with polarization-dependent and time-resolved two-photon interference *Phys. Rev. Lett.* **114** 010401
[14] Du S, Kolchin P, Belthangady C, Yin G Y and Harris S E 2008 Subnatural linewidth biphotons with controllable temporal length *Phys. Rev. Lett.* **100** 183603

[15] Zhao L, Guo X, Liu C, Sun Y, Loy M M T and Du S 2014 Photon pairs with coherence time exceeding 1 μs *Optica* **1** 84–88
[16] Han Z, Qian P, Zhou L, Chen J F and Zhang W 2015 Coherence time limit of the biphotons generated in a dense cold atom cloud *Scientific Reports* **5** 9126
[17] Olislager L, Cussey J, Nguyen A T, Emplit P, Massar S, Merolla J-M and Phan Huy K 2010 Frequency-bin entangled photons *Phys. Rev.* A **82** 013804
[18] Kimble H J 2008 The quantum internet *Nature* **453** 1023–30